NANO LETTERS

2007
Vol. 7, No. 6
1793−1798

Photosensitization of ZnO Nanowires with CdSe Quantum Dots for Photovoltaic Devices

Kurtis S. Leschkies,[†] Ramachandran Divakar,[†] Joysurya Basu,[†] Emil Enache-Pommer,[†] Janice E. Boercker,[†] C. Barry Carter,[†] Uwe R. Kortshagen,[‡] David J. Norris,*[,†] and Eray S. Aydil*[,†]

Department of Chemical Engineering & Materials Science, University of Minnesota, 421 Washington Avenue SE, Minneapolis, Minnesota 55455, and Department of Mechanical Engineering, University of Minnesota, 111 Church Street SE, Minneapolis, Minnesota 55455

Received February 22, 2007

ABSTRACT

We combine CdSe semiconductor nanocrystals (or quantum dots) and single-crystal ZnO nanowires to demonstrate a new type of quantum-dot-sensitized solar cell. An array of ZnO nanowires was grown vertically from a fluorine-doped tin oxide conducting substrate. CdSe quantum dots, capped with mercaptopropionic acid, were attached to the surface of the nanowires. When illuminated with visible light, the excited CdSe quantum dots injected electrons across the quantum dot–nanowire interface. The morphology of the nanowires then provided the photoinjected electrons with a direct electrical pathway to the photoanode. With a liquid electrolyte as the hole transport medium, quantum-dot-sensitized nanowire solar cells exhibited short-circuit currents ranging from 1 to 2 mA/cm^2 and open-circuit voltages of 0.5–0.6 V when illuminated with 100 mW/cm^2 simulated AM1.5 spectrum. Internal quantum efficiencies as high as 50–60% were also obtained.

While solar energy could provide enough power to satisfy the current worldwide demand, the fabrication of photovoltaic systems that are efficient and competitive with fossil fuels remains a serious challenge. To solve this problem, new strategies for solar-to-electric energy conversion are under development.[1] Many of these strategies utilize the following sequence of physical processes: (i) a light-absorbing material generates an electron−hole pair, (ii) the electron and hole separate quickly into two different phases, and (iii) the carriers are transported in these respective phases to opposing electrodes. During each of these steps, efficiency requires that charge recombination is minimized. One classic example of such a photovoltaic device is the dye-sensitized solar cell, in which light is absorbed by dye molecules adsorbed at the interface between a network of TiO_2 nanoparticles and a hole-conducting liquid electrolyte.[2−4] Another example is the bulk heterojunction solar cell, in which two immiscible transport materials are blended to form a three-dimensional bicontinuous network.[5−7] In this case, light is absorbed by either phase, but the photogenerated electrons and holes can quickly dissociate into separate phases because the topology dictates that the interfacial boundary is always nearby. Both organic and inorganic materials have been used to demonstrate this approach.[8−13] However, despite the successes of dye-sensitized and bulk heterojunction solar cells, new combinations of materials and device architectures are still sought to improve further the performance and cost of solar cells.

One possibility is the use of semiconductor nanocrystals, known as quantum dots (QDs), in lieu of photosensitive dyes. For example, CdS,[14,15] CdSe,[16−18] InP,[19] and InAs[20] QDs have been combined with mesoscopic networks of TiO_2 nanoparticles to obtain quantum-dot-sensitized solar cells (QDSSCs). In general, QDs offer several significant advantages over dyes.[21] QDs provide the ability to match the solar spectrum better because their absorption spectrum can be tuned with particle size. In addition, it has been shown recently that QDs can generate multiple electron−hole pairs per photon, which could improve the efficiency of the device.[22−25]

A second possibility that has been studied is the use of single-crystal, wide band gap semiconductor nanowires as the electron transport material. Photoelectrodes in which arrays of such nanowires are grown vertically from a conducting substrate are emerging as an alternative to the mesoporous nanocrystalline TiO_2 films in dye-sensitized solar cells.[26−29] The nanowires can help improve electron transport by avoiding the particle-to-particle hopping that occurs in the TiO_2 network. Furthermore, the nanowire morphology

* Corresponding authors. E-mail: aydil@umn.edu and dnorris@umn.edu.
[†] Department of Chemical Engineering & Materials Science.
[‡] Department of Mechanical Engineering.

10.1021/nl070430o CCC: $37.00
Published on Web 05/16/2007

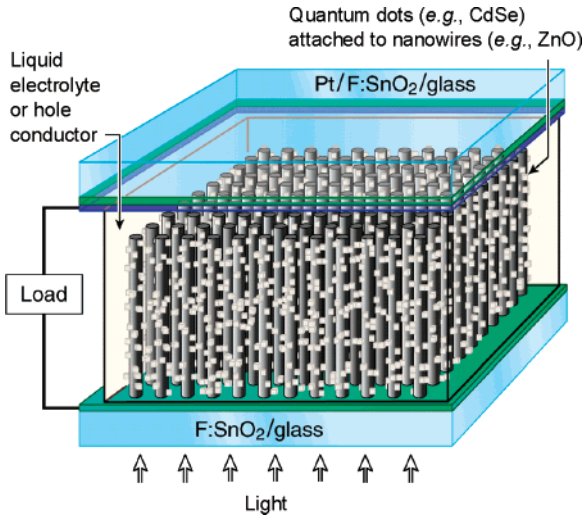

Figure 1. Schematic of the quantum-dot-sensitized solar cell. An array of ZnO nanowires, grown vertically from an F-doped SnO_2/glass substrate and decorated with CdSe quantum dots, serves as the photoanode. A second F-doped SnO_2/glass substrate, coated with a 100 Å layer of Pt, is the photocathode. The space between the two electrodes is filled with a liquid electrolyte, and the cell is illuminated from the bottom, as shown.

can increase the likelihood that all photogenerated electrons have a direct connection to the collection electrode.

Building from these ideas, here we examine the combination of QDs and nanowires in a photovoltaic cell. An array of nanowires photosensitized with QDs should form a particularly promising solar cell architecture. Due to the presence of many nanometer-size heterointerfaces between the semiconductor nanocrystals and the nanowires, it provides significant advantages both for light absorption and for charge separation, two critical steps in solar-to-electric energy conversion. To study this possibility, below we demonstrate photosensitization of ZnO nanowires with CdSe QDs and show evidence for photogenerated electron transfer from the QDs to the nanowires.

Our device configuration, which is depicted in Figure 1, can separate the positive and negative photogenerated carriers into different regions of the solar cell using the following mechanism. After incident photons are absorbed by the QDs, photoexcited electron−hole pairs are confined within the nanocrystal. If they are not separated quickly, they will simply recombine. However, ZnO forms a type II heterojunction with semiconductors such as CdSe. Consequently, once photoexcited, an electron in the QD will lie above the conduction band edge of the ZnO. Thus, the electron can decrease its energy by transferring into the ZnO. This process can occur on a subnanosecond time scale, as has been shown for CdS QDs adsorbed onto a mesoporous TiO_2 nanocrystalline film.[30,31] The presence of a linker molecule between the QD and the ZnO can affect both the electronic structure at the interface and the electron-transfer rate but not the electron energy difference between the QD and the ZnO away from the interface. While electron transfer will still be energetically favorable, the exact mechanism of electron transfer will depend on the linker molecule. For example, in the absence of a resonant charge-transfer mechanism or conjugation in the linker molecule, electron transfer occurs via tunneling and the transfer rate is expected to decrease with increasing linker size (i.e., increased QD-to-ZnO distance). Here, we use short bifunctional molecules of the type X−R−Y, where X and Y are groups that bind to CdSe (X = −SH) and ZnO (Y = −COOH), respectively. Specifically, we use mercaptopropionic acid (MPA), where R is a short carbon chain (R = $-CH_2CH_2-$). After the electron is injected into the ZnO, the positively charged QD can be neutralized either by hole injection into a hole conductor or through an electrochemical reaction with a redox couple in an electrolyte. In either case, the hole level in the QD must be below the highest occupied molecular orbital of the hole conductor or below the redox potential of the redox couple in the electrolyte. The hole then can decrease its energy by leaving the QD.

For this work, we used an electrolyte containing the triiodide/iodide (I_3^-/I^-) redox couple to neutralize the positively charged QDs. It is well-known that electron recombination at the semiconductor−electrolyte interface in dye-sensitized solar cells, which are assembled using this electrolyte, is very slow and photosensitization and electron injection can be studied with minimal interference from high interfacial recombination.[3,32] We utilize this advantage here. However, quantum dots are also known to corrode in this electrolyte and, therefore, QDSSC performance is expected to degrade over time.[32] For example, Zaban et al.[19] reported that n-type InP quantum-dot-sensitized TiO_2 solar cells were unstable in this electrolyte. We have observed similar results for our solar cells, which were stable from several hours to a few days in air. Optimized QDSSCs will require a transition away from a liquid electrolyte to a different hole transport medium, which will be the focus of future work.

To obtain our devices, first we grew ZnO nanowires directly onto transparent and conducting F-doped SnO_2 (FTO) substrates from an aqueous solution of $Zn(NO_3)_2$ and methenamine between 80 and 95 °C.[28,29,33] (Complete experimental details are provided in the Supporting Information.) Figure 2a shows a cross-sectional scanning electron micrograph of typical ZnO nanowires used as photoanodes. Our nanowires have lengths and diameters between 2 and 12 μm and 75 and 125 nm, respectively, and planar densities of 6−40 wires/μm^2.

Separately, we prepared CdSe nanocrystals from CdO according to standard methods.[34] After synthesis, the surfaces of the particles are covered with several different hydrophobic ligands, including tri-*n*-octylphosphine oxide (TOPO), tri-*n*-octylphosphine, and hexadecylamine (HDA). Consequently, the QDs form stable dispersions in nonpolar organic solvents. We then exchanged these ligands with MPA by dispersing the QDs in a mixture of methanol, MPA, and tetramethylammonium hydroxide and refluxing overnight under nitrogen.[35] After this exchange, the QDs were stable in protic solvents but flocculated in nonpolar organic solvents. This observation suggests that the sulfur atom in MPA is bound to the QD surface while the acid group faces the solvent. This conclusion is also consistent with attenuated total internal reflection Fourier transform infrared (ATR-

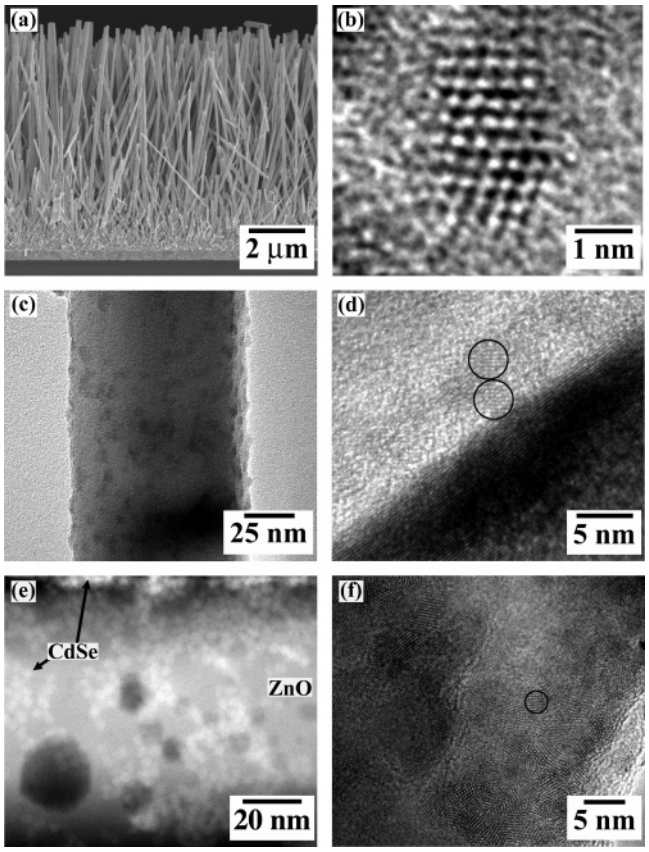

Figure 2. (a) Cross-sectional scanning electron micrograph of ZnO nanowires. (b) High-resolution transmission electron micrograph of a CdSe quantum dot capped with MPA. (c) Bright-field transmission electron micrograph of a ZnO nanowire decorated with CdSe quantum dots. (d) High-resolution transmission electron micrograph of CdSe quantum dots attached to a ZnO nanowire. The location of the quantum dots is outlined as a visual aid. ZnO nanowires in (c) and (d) were not treated with O_2 plasma prior to adsorption of the quantum dots. (e) Scanning transmission electron microscope high-angle annular dark-field image of a ZnO nanowire decorated with CdSe quantum dots. (f) High-resolution transmission electron micrograph of CdSe quantum dots attached to a ZnO nanowire. One of the quantum dots has been outlined. ZnO nanowires in (e) and (f) were treated with O_2 plasma prior to quantum dot adsorption.

FTIR) spectra of the QDs (Figure S1 in the Supporting Information). The presence of COO^- symmetric and asymmetric stretches at 1581 and 1385 cm^{-1}, respectively, and the absence of the S−H stretch indicate that the MPA ligands are deprotonated and bound to the QD surface through the sulfur atoms. The IR spectra also show that tetramethylammonium ions $[N(CH_3)_4]^+$ are associated with the carboxylate anions. The CH_3 stretching and deformation peaks of these quaternary amines are detected at 3023 and 1492 cm^{-1}, respectively. The P═O and N−H bands characteristic of adsorbed TOPO and HDA, both of which were present in the IR spectra of QDs before the MPA exchange (Figure S2), are not observed in Figure S1. This indicates that, within our detection limit, all of the TOPO and HDA ligands were replaced with MPA.

Figure 2b shows a high-resolution transmission electron micrograph (HRTEM) of a MPA-capped CdSe QD isolated from a colloidal suspension. TEM images of ensembles of our QDs indicate that the QDs are single crystals with diameters ranging from 3 to 4 nm. Energy dispersive X-ray (EDX) spectra of these QDs show signal for S, consistent with MPA adsorbed on their surfaces.

Such MPA-capped CdSe QDs were attached to ZnO by immersing the nanowire-coated substrates in a dispersion of QDs in methanol. The QDs could attach to the ZnO surfaces via the carboxylate groups.[36] Figure 2c shows a bright-field TEM image of a ZnO nanowire decorated with an ensemble of CdSe QDs. The QDs are visible as the circular dark spots on the surface of the nanowire and EDX confirms that they are CdSe. A HRTEM image of the nanowire edge (Figure 2d) provides more compelling evidence that QDs are attached to the nanowire surface. An abrupt transition is observed between the $(10\bar{1}0)$ lattice planes of the ZnO nanowire and the (111) lattice planes of the CdSe QD, indicating an intimate contact between the QD and the nanowire within an approximate distance of 0.29 nm, or one ZnO $(10\bar{1}0)$ lattice spacing. However, these TEMs also show that the QD coverage on the nanowires is low.

CdSe QD coverage on the nanowires was significantly increased by treating the nanowire-coated substrates with oxygen plasma before they were immersed in the colloidal dispersion. Figure 2e shows a scanning transmission electron microscope (STEM) image of a CdSe QD-decorated ZnO nanowire that was treated with oxygen plasma before adsorption of the QDs. The STEM image was obtained using a high-angle annular dark-field detector which is sensitive to the atomic number contrast between the CdSe QDs and the underlying ZnO nanowire; the image intensity is proportional to the average square of the atomic numbers of the elements in the material and, as a result, the QDs appear as circular bright spots on the nanowire surface and along the nanowire edges. (We attribute the large dark circles on the left-hand side of the image to organic contamination.) Figure 2f shows a HRTEM image of the edge of a plasma-treated nanowire where one of the QDs has been outlined. The attached QDs appear as randomly oriented crossed-fringe patterns on the nanowire surface. In all samples examined under TEM, the QDs coat the surface of the plasma-treated nanowires (parts e and f of Figure 2) while untreated nanowires show significantly lower QD coverage after QD adsorption (parts c and d of Figure 2). Additional HRTEM images are provided in the Supporting Information to illustrate further the advantage of the oxygen plasma treatment.

The oxygen plasma may modify the ZnO nanowire surface in a number of ways to enhance QD adsorption. For example, the oxygen plasma can charge the nanowire surface, create dangling bonds through ion bombardment, and/or remove surface contaminants. While it is difficult to identify the effect of the plasma on the ZnO nanowire surface with certainty, ATR-FTIR spectra of the ZnO nanowires recorded after plasma exposure suggest that surface-bound contaminants are removed from their surfaces (Figure S4 in the Supporting Information). In particular, the absorbance reduction observed at 3240 cm^{-1} (associated O−H stretching modes) and 2960, 2931, and 2858 cm^{-1} (C−H stretching

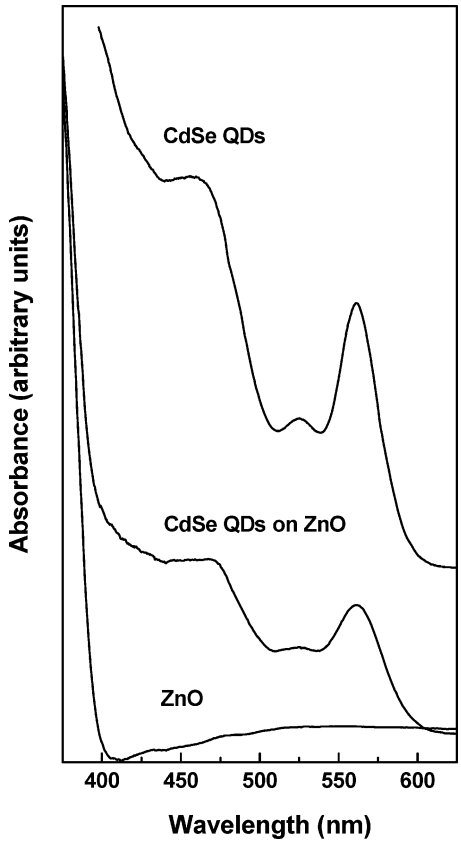

Figure 3. Room-temperature optical absorption spectra of a dispersion of ~3 nm MPA-capped CdSe QDs in methanol and a 2 μm long ZnO nanowire-coated FTO substrate before and after adsorption with the same QDs. The QD absorbance spectrum is shifted along the *y*-axis for clarity. The small finite absorbance of the ZnO nanowires at wavelengths greater than 400 nm for the bare nanowire substrate is an artifact due to reduced light scattering from the ZnO nanowires at longer wavelengths.

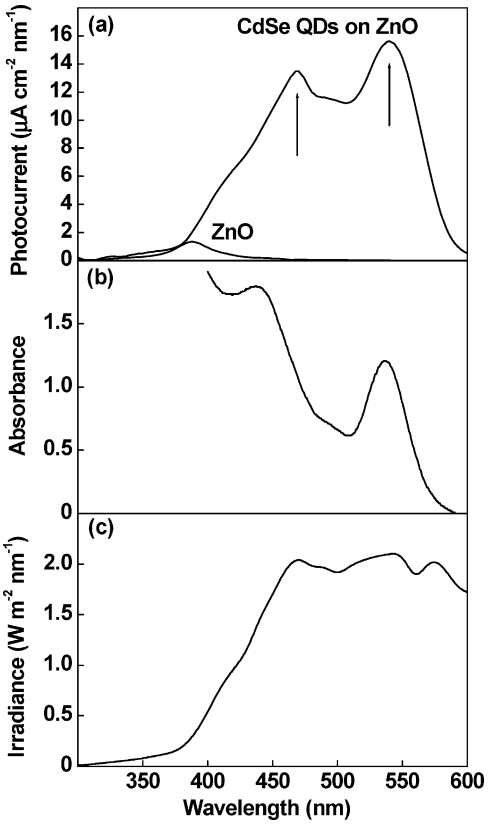

Figure 4. (a) Room-temperature photocurrent action spectrum of solar cells assembled using CdSe-QD-sensitized and unsensitized nanowires. (b) Room-temperature optical absorption spectrum of the MPA-capped CdSe QDs used as photosensitizers for the QDSSC tested in (a). (c) Irradiance spectrum of the simulated AM1.5 light source used for testing the QDSSC in (a). The slit at the entrance of the monochromator was adjusted to give a ~10 nm bandpass.

modes) correspond to the removal of surface hydroxyl and hydrocarbon groups, respectively. Such surface species may prevent the colloidal QDs from attaching to the nanowire surface through the carboxyl group, and higher surface coverage is obtained when these species are removed.

The optical absorption properties of the CdSe QDs were preserved when the QDs were attached to the ZnO nanowires. For example, Figure 3 shows the absorption spectrum of ~2 μm long ZnO nanowires before and after sensitization with ~3 nm diameter MPA-capped CdSe QDs. These nanowire spectra were obtained from diffuse reflectance measurements using an integrating sphere. (The reflectance spectrum of an uncoated F-doped SnO_2 substrate was used as reference.) When the QDs were attached to the nanowires, features at 465, 526, and 562 nm appeared due to the size-dependent electronic transitions in the CdSe. The shape of these absorption features is identical to that observed in the absorption spectrum of MPA-passivated CdSe QDs dispersed in methanol.

Finally, we assembled quantum-dot-sensitized nanowire solar cells by placing a QD-decorated nanowire photoanode face-to-face with an F-doped SnO_2 photocathode coated with a thin layer of Pt (~100 Å). The two parallel electrodes were separated using Teflon spacers and clamped together. The space between the electrodes (~25 μm) was filled through capillary action with the electrolyte (0.05 M I_2, 0.5 M 4-*tert*-butylpyridine, and 0.5 M LiI in short chain hydrocarbons).

Photocurrent action spectra and solar cell current−voltage ($I-V$) characteristics were recorded using a Xe-arc lamp in conjunction with a monochromator. The monochromator is equipped with both a grating and a high reflectivity mirror mounted on the same turret. This arrangement allows us to illuminate our cells with either the broadband AM1.5 spectrum (using the mirror) or a selected wavelength range from this spectrum (using the grating). The AM1.5 spectrum was generated using commercially available filters (Newport Corp.) between the Xe-arc lamp and the monochromator; the filters were designed to simulate the solar spectrum when used in conjunction with this lamp.

When illuminated, our devices exhibit the photovoltaic effect and clear evidence for electron injection into the nanowires from excited CdSe QDs. For example, Figure 4a shows the photocurrent action spectrum of a QDSSC prepared using ~12 μm long plasma-treated ZnO nanowires and ~3 nm diameter MPA-capped CdSe QDs. The photocurrent spectrum for an unsensitized nanowire solar cell assembled using ~12 μm long ZnO nanowires is also shown in Figure 4a for comparison. The unsensitized solar cell generates very little photocurrent for wavelengths longer than

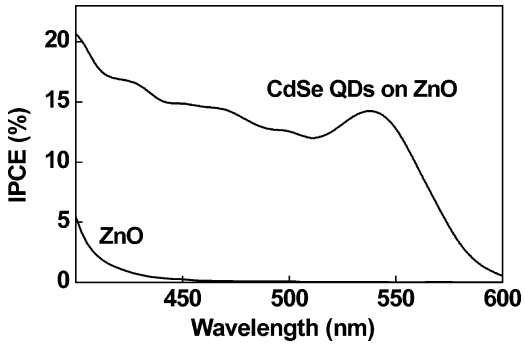

Figure 5. IPCE spectrum of the quantum-dot-sensitized and unsensitized ZnO nanowire solar cell featured in Figure 4a.

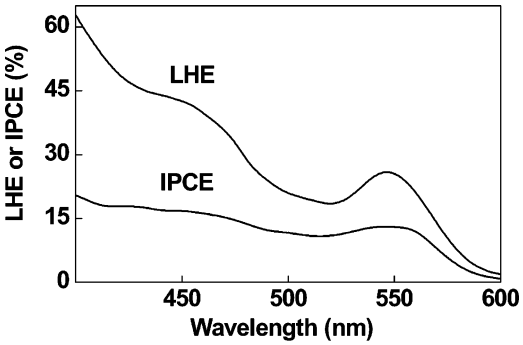

Figure 6. IPCE and LHE spectra of a quantum-dot-sensitized solar cell. Division of IPCE by LHE gives the product of injection and collection efficiencies or the internal quantum efficiency (IQE).

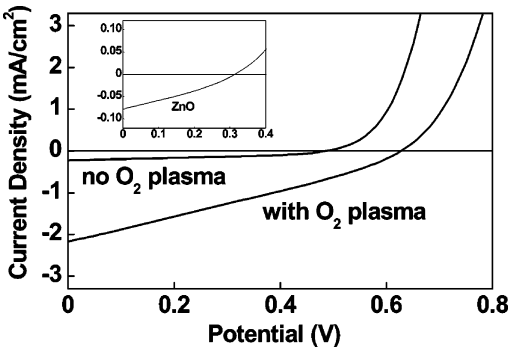

Figure 7. Current−voltage ($I-V$) characteristics of QDSSCs assembled using plasma-treated and untreated ZnO nanowires. The $I-V$ characteristics were recorded while illuminating the solar cells with 100 mW/cm^2 simulated AM1.5 spectrum. The inset shows the $I-V$ characteristics of an unsensitized ZnO nanowire solar cell. The units of the inset are the same as the large figure. The fill factor of the unsensitized nanowire solar cell is 0.27.

400 nm, which are below the band gap of ZnO. In contrast, the QDSSC shows a much larger photocurrent between 400 and 600 nm, where the CdSe QDs absorb. In fact, the shape of the photocurrent spectrum, with its two peaks at 470 and 540 nm (shown with arrows), resembles that of the QD optical absorption spectrum, shown in Figure 4b. Differences, such as the decreasing photocurrent for wavelengths shorter than 450 nm and the small red shift of the absorption peak at 441 nm to 470 nm in the photocurrent, can be explained by the excitation spectrum (Figure 4c). A calculation of the wavelength dependence of the photocurrent using the QDSSC absorption spectrum and the simulated AM1.5 excitation source reproduces the shape of the measured action spectrum. Thus, we conclude that the additional photocurrent generated in the visible region of the spectrum is due to electron−hole pairs photoexcited in the QDs followed by injection of electrons to the ZnO nanowires.

Figure 5 shows the wavelength dependence of the incident photon-to-current conversion efficiency (IPCE, also called external quantum efficiency) for the QDSSC and the unsensitized nanowire solar cell featured in Figure 4a. The IPCE of the QDSSC shows a clearly resolved peak at 540 nm which aligns exactly with the position of the first excited state in the CdSe. The remaining CdSe excitonic structure is smeared for wavelengths shorter than 500 nm when the photocurrent spectrum is divided by the product of the excitation spectrum and wavelength to obtain the IPCE.

Light harvesting efficiency (LHE) and IPCE measurements indicate that the internal quantum efficiency (IQE = IPCE/LHE) of the QDSSCs are comparable to those in dye-sensitized ZnO nanowire solar cells,[26−28] and that the overall power conversion efficiency is limited by the surface area of the nanowires. Figure 6 shows the IPCE and LHE spectra of a QDSSC assembled using ∼10 μm long ZnO nanowires pretreated with oxygen plasma and decorated with ∼3 nm diameter MPA-capped CdSe QDs. The internal quantum efficiency of this QDSSC in the spectral range covering the first excitonic transition (∼500−600 nm) is 50−60%, comparable to those reported for dye-sensitized solar cells made using similar nanowires.[26−28] For this particular solar cell architecture, the IQE is the product of the efficiency of electron injection from the QD to the nanowire and the collection efficiency of photoinjected electrons. Thus, 50−60% is also a lower bound on the electron injection efficiency. While an approximate factor of 2 improvement in IQE is possible, these measurements indicate that the overall power conversion efficiency of the QDSSCs is largely limited by the LHE and the surface area of the nanowires available for QD adsorption. Indeed, this is the same limitation as observed with ZnO nanowire dye-sensitized solar cells.[26−28]

Figure 7 shows $I-V$ characteristics of two QDSSCs recorded during illumination with 100 mW/cm^2 simulated AM1.5 spectrum. One of these cells was assembled using a ZnO nanowire electrode that was treated with oxygen plasma while the electrode for the second cell was not treated. The $I-V$ characteristic for an unsensitized nanowire solar cell is also shown in the inset of Figure 7 for comparison. All of these cells were assembled using photoanodes with ∼12 μm long ZnO nanowires. Both the power conversion efficiency (0.4%) and the short-circuit current (2.1 mA/cm^2) of the QDSSC assembled using nanowires treated with an oxygen plasma are more than an order of magnitude higher than those obtained for the QDSSC assembled using nanowires that were not plasma treated. This result is consistent with TEM images shown in Figure 2c−f: the higher QD coverage obtained with oxygen plasma-treated nanowires results in increased light absorption and higher photocurrent. Typical QDSSCs assembled with ∼12 μm long plasma-treated ZnO

nanowires had short-circuit currents ranging from 1 to 2 mA/cm^2 and open-circuit voltages of 0.5−0.6 V with a fill factor of ∼0.3.

In summary, we have demonstrated a quantum-dot-sensitized nanowire solar cell based on photosensitization of ZnO nanowires with CdSe quantum dots. Photocurrent is generated from visible light by the excitation of electron−hole pairs in the CdSe quantum dots. The electrons are injected across the quantum dot−nanowire interface into the ZnO, a process that is facilitated by the overlap between the electronic states in the quantum dot and the ZnO conduction band. The morphology of the nanowires provides the photoinjected electrons with a direct electrical pathway to the photoanode. While here we have focused on the electron transfer from CdSe quantum dots to ZnO nanowires, further improvement on the efficiency and stability of these devices will require development of an optimal hole transport medium for this architecture. QDSSCs such as those described herein provide additional opportunities that are not available with dye-sensitized solar cells. First, the use of quantum dots in lieu of the dye allows for the ability to tune the optical absorption in the solar cell through selection of semiconductor material and particle size. Second, QDSSCs can potentially exploit the recently observed multiple electron−hole pair generation per photon to achieve higher efficiencies[37,38] than that predicted by Shockley and Queisser.[39]

Acknowledgment. This work was supported by the NSF under the NIRT program (CTS-0506672) and the Minnesota Initiative for Renewable Energy and the Environment (IREE, LG-C5-2005). We utilized the University of Minnesota Characterization Facility which receives partial support from the NSF under the NNIN program. K.S.L. was supported by the IGERT program of the NSF (DGE-0114372). R.D. was supported in part by the MRSEC program of the NSF (DMR-0212302). C.B.C. and J.B. extend thanks to the 3M Helzer Endowment fund. D.J.N. acknowledges support from the Alexander von Humboldt Foundation. We thank S. Agarwal for assistance.

Supporting Information Available: Detailed experimental methods, ATR-FTIR spectra, and TEM images. This information is available free of charge via the Internet at http://pubs.acs.org.

References

(1) Gregg, B. A. *J. Phys. Chem. B* **2003**, *107*, 4688.
(2) O'Regan, B.; Gratzel, M. *Nature* **1991**, *335*, 737.
(3) Gratzel, M. *Nature* **2001**, *414*, 338.
(4) Durr, M.; Bamedi, A.; Yasuda, A.; Nelles, G. *Appl. Phys. Lett.* **2004**, *84*, 3397.
(5) Sariciftci, N. S.; Braun, D.; Zhang, C.; Srdanov, V. I.; Heeger, A. J.; Stucky, G.; Wudl, F. *Appl. Phys. Lett.* **1993**, *62*, 585.
(6) Yu, G.; Gao, J.; Hummelen, J. C.; Wudl, F.; Heeger, A. J. *Science* **1995**, *270*, 1789.
(7) Huynh, W. U.; Dittmer, J. J.; Alivisatos, A. P. *Science* **2002**, *295*, 2425.
(8) Greenham, N. C.; Peng, X. G.; Alivisatos, A. P. *Phys. Rev. B* **1996**, *54*, 17628.
(9) Coakley, K. M.; McGehee, M. D. *Appl. Phys. Lett.* **2003**, *83*, 3380.
(10) Huynh, W. U.; Dittmer, J. J.; Libby, W. C.; Whiting, G. L.; Alivisatos, A. P. *Adv. Funct. Mater.* **2003**, *13*, 73.
(11) Coakley, K. M.; Liu, Y. X.; McGehee, M. D.; Frindell, K. L.; Stucky, G. D. *Adv. Funct. Mater.* **2003**, *13*, 301.
(12) Coakley, K. M.; McGehee, M. D. *Chem. Mater.* **2004**, *16*, 4533.
(13) Gur, I.; Fromer, N. A.; Geier, M. L.; Alivisatos, A. P. *Science* **2005**, *310*, 462.
(14) Vogel, R.; Hoyer, P.; Weller, H. *J. Phys. Chem.* **1994**, *98*, 3183.
(15) Vogel, R.; Pohl, K.; Weller, H. *Chem. Phys. Lett.* **1990**, *174*, 241.
(16) Liu, D.; Kamat, P. *J. Phys. Chem.* **1993**, *97*, 10769.
(17) Robel, I.; Subramanian, V.; Kuno, M.; Kamat, P. V. *J. Am. Chem. Soc.* **2006**, *128*, 2385.
(18) Niitsoo, O.; Sarkar, S. K.; Pejoux, C.; Ruhle, S.; Cahen, D.; Hodes, G. *J. Photochem. Photobiol., A* **2006**, *181*, 306.
(19) Zaban, A.; Micic, O. I.; Gregg, B. A.; Nozik, A. J. *Langmuir* **1998**, *14*, 3153.
(20) Yu, P.; Zhu, K.; Norman, A. G.; Ferrere, S.; Frank, A. J.; Nozik, A. J. *J. Phys. Chem. B* **2006**, *110*, 25451.
(21) Nozik, A. J. *Physica E* **2002**, *14*, 115.
(22) Schaller, R. D.; Klimov, V. I. *Phys. Rev. Lett.* **2004**, *92*, 186601.
(23) Ellingson, R. J.; Beard, M. C.; Johnson, J. C.; Yu, P. R.; Micic, O. I.; Nozik, A. J.; Shabaev, A.; Efros, A. L. *Nano Lett.* **2005**, *5*, 865.
(24) Schaller, R. D.; Petruska, M. A.; Klimov, V. I. *Appl. Phys. Lett.* **2005**, *87*, 253102.
(25) Murphy, J. E.; Beard, M. C.; Norman, A. G.; Ahrenkiel, S. P.; Johnson, J. C.; Yu, P. R.; Micic, O. I.; Ellingson, R. J.; Nozik, A. J. *J. Am. Chem. Soc.* **2006**, *128*, 3241.
(26) Baxter, J. B.; Aydil, E. S. *Appl. Phys. Lett.* **2005**, *86*, 053114.
(27) Baxter, J. B.; Aydil, E. S. *Solar Energy Mater. Solar Cells* **2006**, *90*, 607.
(28) Baxter, J. B.; Walker, A. M.; van Ommering, K.; Aydil, E. S. *Nanotechnology* **2006**, *17*, S304.
(29) Law, M.; Greene, L. E.; Johnson, J. C.; Saykally, R.; Yang, P. D. *Nat. Mater.* **2005**, *4*, 455.
(30) Evans, J. E.; Springer, K. W.; Zhang, J. Z. *J. Chem. Phys.* **1994**, *101*, 6222.
(31) Blackburn, J. L.; Selmarten, D. C.; Nozik, A. J. *J. Phys. Chem. B* **2003**, *107*, 14154.
(32) Gratzel, M. *J. Photochem. Photobiol., C* **2003**, *4*, 145.
(33) Greene, L. E.; Law, M.; Goldberger, J.; Kim, F.; Johnson, J. C.; Zhang, Y. F.; Saykally, R. J.; Yang, P. D. *Angew. Chem., Int. Ed.* **2003**, *42*, 3031.
(34) Reiss, P.; Bleuse, J.; Pron, A. *Nano Lett.* **2002**, *2*, 781.
(35) Aldana, J.; Wang, Y. A.; Peng, X. G. *J. Am. Chem. Soc.* **2001**, *123*, 8844.
(36) Westermark, K.; Rensmo, H.; Lees, A. C.; Vos, J. G.; Siegbahn, H. *J. Phys. Chem. B* **2002**, *106*, 10108.
(37) Klimov, V. I. *Appl. Phys. Lett.* **2006**, *89*, 123118.
(38) Hanna, M.; Nozik, A. J. *J. Appl. Phys.* **2006**, *100*, 074510.
(39) Shockley, W.; Queisser, H. J. *J. Appl. Phys.* **1961**, *32*, 510.

NL070430O